Materials Characterization 205 (2023) 113268

Contents lists available at ScienceDirect

Materials Characterization

journal homepage: www.elsevier.com/locate/matchar

Microstructure evolution of a forged TiAl-Nb alloy during high-temperature tensile testing

Shunke Zhang [a,b], Ning Tian [a,b,*], Jianghua Li [c], Guanghua Yang [b], Wenkun Yang [b], Guangyan Wang [a,b], Zhanqi Liu [d], Yongxiang Li [b]

[a] Guizhou Communications Polytechnic, Guiyang 551400, China
[b] Guizhou University of Engineering Science, Bijie 551700, China
[c] Institute of Mechanics, Chinese Academy of Sciences, Beijing 100190, China
[d] Liaoning University of Technology, Jinzhou 121001, China

ARTICLE INFO

Keywords:
TiAl-Nb alloy
High-temperature tensile
Brittle-ductile transition
Deformation mechanism

ABSTRACT

A forged TiAl-Nb alloy was investigated by means of measurements of properties related to performance at high temperatures, and the microstructure was observed by scanning electron microscopy (SEM) with electron backscattering diffraction (EBSD) and transmission electron microscopy (TEM). The brittle-ductile transition temperature of the alloy was between 800 °C and 820 °C. The alloy had high strength in the brittle stage, and the main deformation mechanisms of the alloy were dislocation movement and dynamic recovery (DRV) in the γ phase. In the ductile stage, the alloy had good deformation ability and the main deformation mechanism of the alloy was continuous dynamic recrystallization (CDRX) in γ phase and α_2 phase, the integrity of the lamellar colonies was destroyed. At the same time, the phase transformation occurred.

1. Introduction

TiAl alloys have good potential for applications in the field of high-temperature materials. However, as they are intermetallic compounds, brittleness at room temperature and poor thermal working properties limit their application [1–3]. Researchers usually overcome the brittleness of TiAl alloys by hot deformation, alloying and heat treatment. The principle is to change the phase structure of alloys to introduce a plastic phase with better properties [4–7].

As-cast TiAl alloys have coarse grain size, nonuniform structure, tendency to undergo segregation, and poor resistance to ductile fracture, and thus they have high requirements for hot deformation processes. Researchers usually refine the organization of as-cast TiAl and improve its machinability by first processing and then secondary processing to obtain final products. Common primary processing technologies include isothermal forging, conventional canned forging and extrusion [8–11], while secondary processing technologies include sheet rolling, superplastic forming and isothermal closed-die forging [12,13]. In recent years, more and more researchers have focused on the dynamic recovery and recrystallization of TiAl alloys [14]. Shi et al. prepared a TiAl-based alloy with superplasticity at 1125–1275 °C by pulsed current-assisted forging, and the study showed that the deformability of the alloy was mainly related to dynamic recrystallization and phase transition [15]. Cui et al. studied the effect of multidirectional forging on the microstructure evolution and tensile properties of TiAl alloy and concluded that the process could refine the microstructure and effectively improve the tensile properties of the alloy [16]. Bystrzanowski et al. studied the microstructure evolution of a Ti-46Al-9Nb alloy during a high-temperature tensile process. They found that mechanical twins and deformation bands were the main deformation characteristics below 850 °C, and dynamic recrystallization was the main deformation characteristic above 850 °C [17].

The brittle-ductile transition (BDT) is a common property of crystalline materials. It refers to the transition from a brittle state with little or no plasticity to a ductile state with more than 10% plastic deformation as the temperature increases [18]. With further research, researchers found that the brittle and ductile transition is closely related to microstructure evolution, mechanical twinning, dislocation slip, deformation zone and dynamic recrystallization [19–21].

The forging process of TiAl alloy is very complicated, and the forged microstructure is closely related to the original microstructure, chemical components, phase composition and thermal processing parameters.

* Corresponding author at: Guizhou Communications Polytechnic, Guiyang 551400, China.
E-mail address: 18640022878@163.com (N. Tian).

https://doi.org/10.1016/j.matchar.2023.113268
Received 12 May 2023; Received in revised form 2 August 2023; Accepted 21 August 2023
Available online 22 August 2023

The structure of the forged alloy is complicated and has high research value. Therefore, in this study, a TiAl-Nb alloy with high performance was prepared by isothermal forging. The deformation mechanism of the alloy was investigated for different tensile temperatures by tensile property tests and microstructure observations. The paper attempts to obtain the high temperature plastic deformation law of forged TiAl alloy, and further deepen the understanding of the internal relationship and law between the microstructure and plastic deformation behavior of forged TiAl alloy, so as to provide a reliable basis for effectively controlling the hot working technology of the material and improving its quality and properties.

2. Experimental materials and methods

The alloy ingot composed of Ti-44Al-8Nb-0.2 W-0.2B-0.1Y (at. %) was isothermally forged at 1250 °C. The isothermal forging process was as follows: After heating the mould to slightly above the forging temperature, the ingot was placed in the mould cavity and then heated to make the temperature of the mould and ingot equal. When the forging temperature was reached, pressure was applied to deform the alloy billet at a low strain rate of 80%. Then, the ingot billet in the isothermal forging state was processed into a sample billet with dimensions 14 mm × 20 mm × 40 mm by wire cutting.

The alloy samples were processed into sheet tensile specimens with a cross section of 4.5 mm × 2.5 mm and a standard distance of 20 mm by wire cutting technology. After mechanical grinding and polishing, WDW-100 electronic universal testing machine was used to measure the tensile properties of the alloy at different temperatures at a rate of 1×10^{-3}/s. The microstructure of the original and tensile fractured samples was observed by SEM (Themo Anre S) and TEM (Talos F200X).

3. Experimental results and analysis

3.1. Microstructure of the forged alloy

The original microstructure of the forged TiAl-Nb alloy observed by electron backscattering diffraction (EBSD) is shown in Fig. 1. Fig. 1(a) and Fig. 1(b) show the IQ map and phase map, respectively. The alloy was composed of lamellar colonies and equiaxed grains. The lamellar colonies were composed of alternating γ lamellae and α_2 lamellae, and the equiaxed grains were composed of larger γ grains and smaller α_2 grains. Figure (b) shows that the fractions of the γ phase, α_2 phase and β(B2) phase were 91.9%, 8.1% and 0.1%, respectively. Compared with the γ phase, the volume fraction of the α_2 phase was smaller.

Fig. 2(a) shows the bright-field TEM images of the interfacial area between the larger lamellar colonies and the smaller lamellar colonies. The larger lamellar colonies showed slight bending deformation, as shown by the white arrow on the left, while the smaller lamellar colonies were not deformed, as shown by the black arrow on the right. Fig. 2(b) shows the enlarged TEM image of the smaller lamellar colony, and the EDS spectrum of Al is shown in the lower left corner. The bright contrast phase with a higher atomic fraction of Al was γ-TiAl phase, and the dark contrast phase with a lower atomic fraction of Al was the α_2-Ti_3Al phase. All the lamellar colony and equiaxed grains were composed of γ-TiAl and α_2-Ti_3Al phases, and the smaller lamellae were relatively straight. Fig. 2(c) shows a TEM image of a large region of lamellae; some lamellae were slightly bent and deformed, as shown by the white arrow in Fig. 2 (c). Fig. 2(d) shows a TEM image of equiaxed grains, where the dark contrast was the γ phase and the light contrast was the α_2 phase. The γ grains in this region were mostly equiaxial and large, and the α_2 grains were irregular in shape and distributed around γ grains, which was consistent with the EBSD observations. Dislocations occurred in some γ grains and plugged into the interface between grains, as shown by the white arrow in Fig. 2(d). No dislocations were observed in the α_2 grains.

3.2. Tensile curves of the forged TiAl-Nb alloy

The tensile curves of the forged TiAl-Nb alloy at 760 °C–840 °C are shown in Fig. 3(a). When the tensile test temperature ranged from 760 °C to 800 °C, the stress increased sharply with increasing elongation, and fracture occurred in a short time. The alloy had high yield strength and low elongation, showing obvious characteristics of brittle fracture. This kind of tensile curve was dynamic recovery type curve. As can be seen from the curve in the figure, the process was divided into two stages: In the first stage, dislocation increment occured in the material structure, and the dislocation increased rapidly with the increase of deformation and shape variable, resulting in the increased of stress. In the second stage, the material had yield deformation, and with the increased of deformation, the work hardening rate decreased, and the dislocation become entangled and multiple changes.

When the temperature exceeded 800 °C, the yield strength decreased sharply, the elongation increased sharply, and the alloy exhibited obvious characteristics of ductile fracture. This kind of tensile curve was a dynamic recrystallization type curve. As can be seen from the curve in the figure, the process was also divided into two stages: In the first stage, as the amount of deformation increased, the hardening was intensified, and at the same time, a substructure was formed to soften the material. At this stage, the hardening action was greater than the softening action, so the stress continued to increase until the peak. In the second stage, as the amount of deformation continued to increase, recrystallization occured, and the stress decreased rapidly.

The yield strength and elongation of the material at different temperatures were compared, as shown in Fig. 3(b). The brittle-ductile transition temperature of the material was between 800 °C and 820 °C.

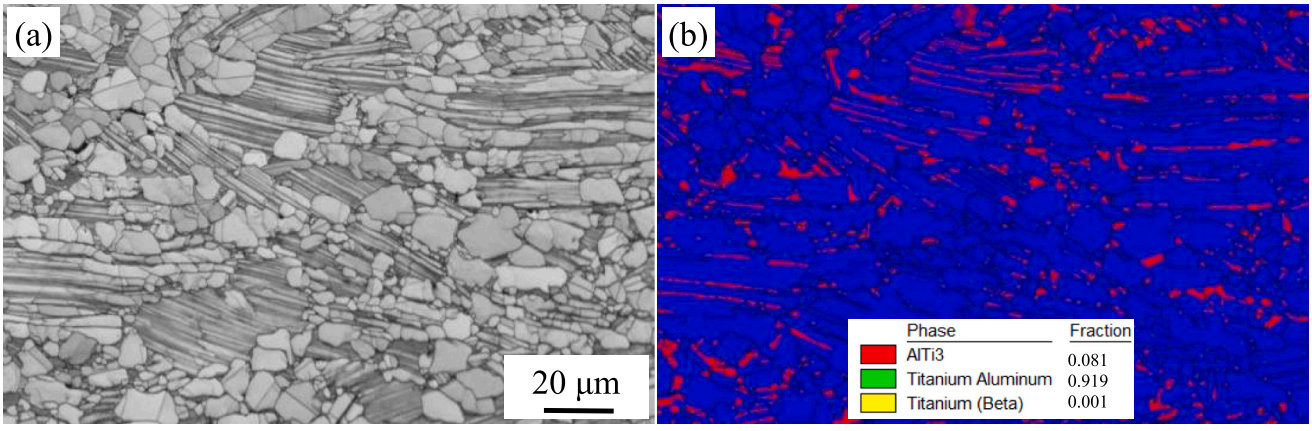

Fig. 1. EBSD observations of the forged high Nb-TiAl alloy: (a) IQ map; (b) phase map.

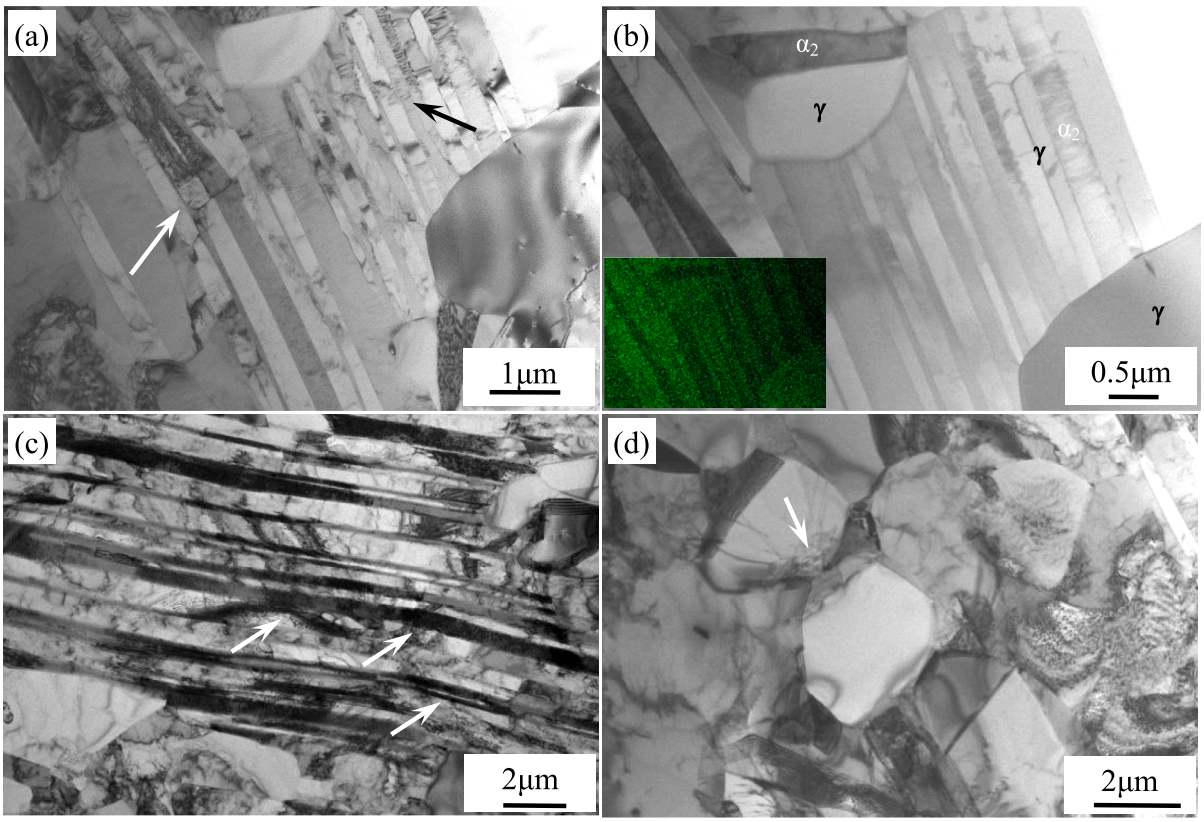

Fig. 2. TEM images of the forged TiAl-Nb alloy: (a) the interface between a region of larger lamellar colony and a smaller lamellar colony; (b) TEM image and EDS pattern of a smaller lamellar colony; (c) TEM image of a larger lamellar colony; (d) TEM image of equiaxed grains.

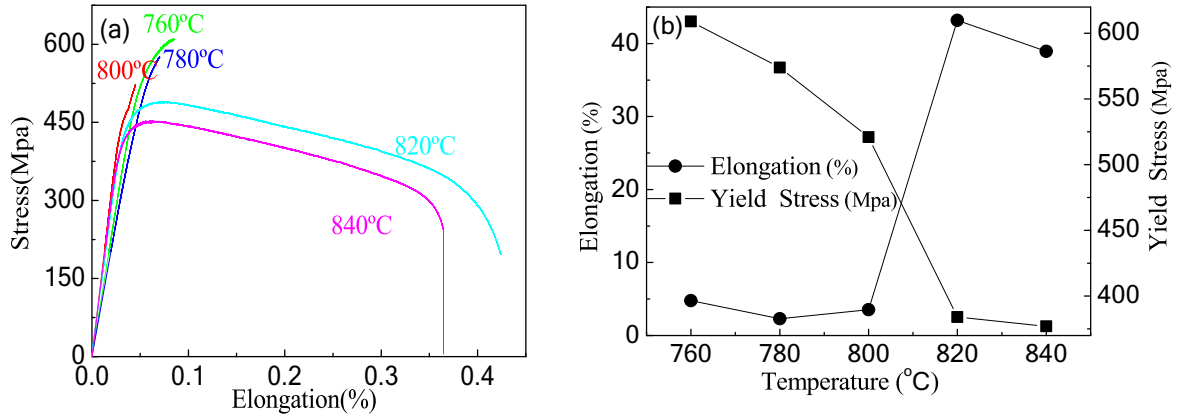

Fig. 3. Relationship between tensile properties and temperature of alloy: (a) stress as a function of elongation; (b) stress as a function of temperature.

3.3. Deformation characteristics of alloys in the brittle stage

The brittle-ductile transition temperature is the main parameter used to characterize the service temperature of alloys, and the high-temperature strength of the alloy in the brittle stage determines the service temperature of the alloy. Fig. 4 shows the EBSD image analysis of tensile fracture of the forged TiAl-Nb alloy at 780 °C (brittle stage). Figs. 4(a)-(b) show the IPF+ grain boundary map and phase map of the alloy, respectively. After tensile fracture at 780 °C, the alloy was still composed of equiaxed grains and lamellar colonies, and no obvious deformation occurred in the lamellar colonies. Small-angle grain boundaries appeared in some of the larger γ grains, accounting for approximately 16.7%, which was attributed to the substructure formed by dislocation entanglement during the tensile process of the alloy. This indicates that a dynamic recovery (DRV) occurs during the tensile process. In the local region, new grains formed through recrystallization inside γ grains, and the orientations of the new grains were different from the original grain orientations, as shown by the black circle in Fig. 4(a). Fig. 4(c) shows the KAM + large-angle grain boundary map of the alloy; the KAM values were small and unevenly distributed. The small-angle grain boundary was substructure formed by dislocation entanglement during the DRV, the distortion was large. Therefore, the KAM value was higher at the location of the small-angle grain boundary.

To further analyse the microstructure transformation and deformation mechanism of the forged TiAl-Nb alloy during the tensile process, TEM analysis of the forged TiAl-Nb alloy after tensile fracture was performed. The TEM images of the alloy near the fracture after tensile fracture at 780 °C are shown in Fig. 5.

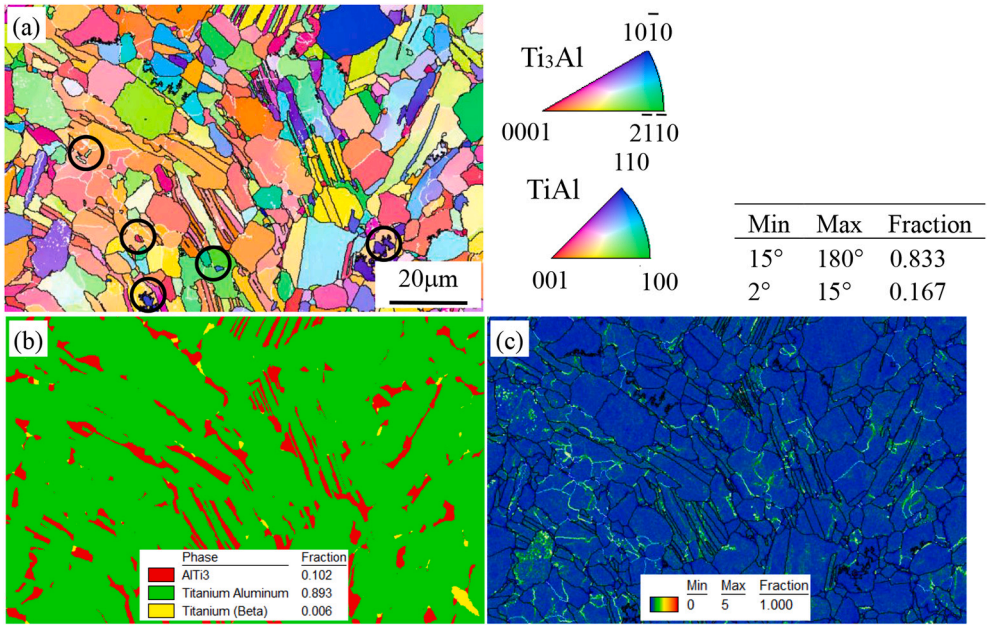

Fig. 4. EBSD observations of the forged alloy near the fracture after tensile fracture at 780 °C: (a) IPF+ grain boundary map; (b) phase map; (c) KAM + large-angle grain boundary map.

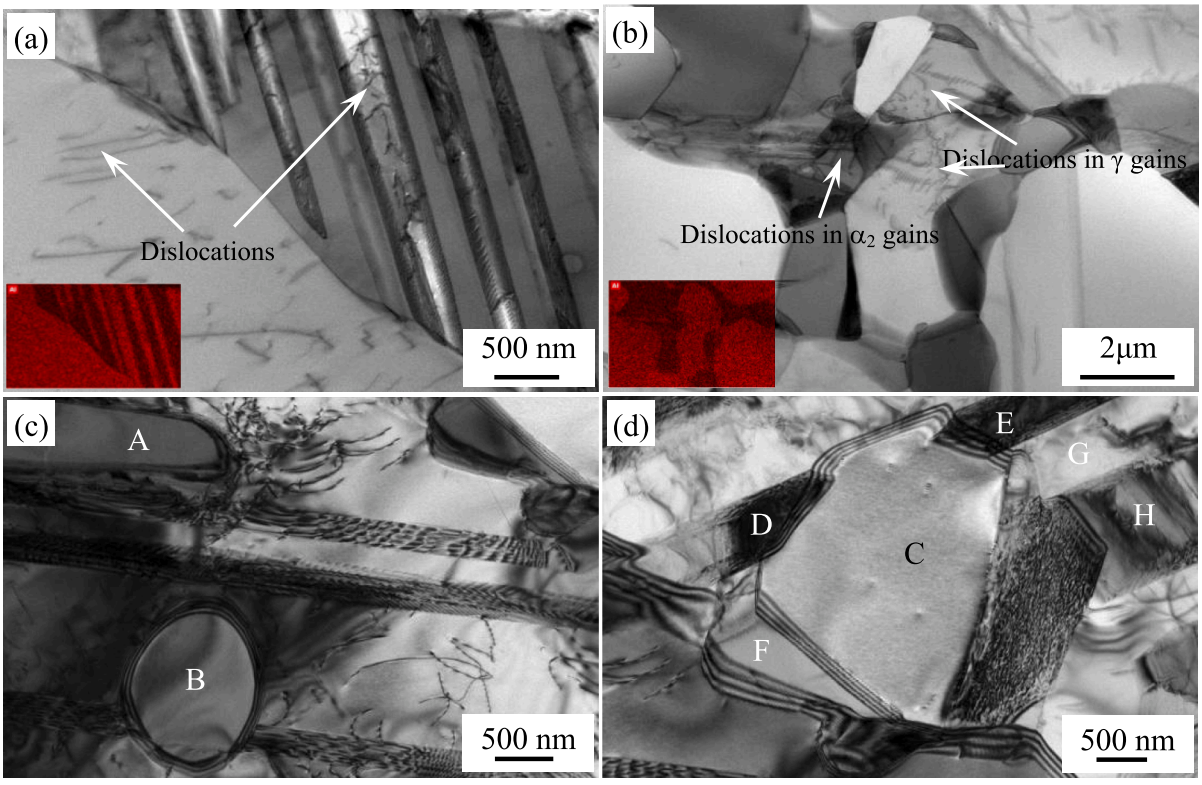

Fig. 5. Deformation features of the forged alloy at 780 °C: (a) boundary between the region of equiaxed grains and the region of lamellae; (b) microstructure of the region of equiaxed grains; (c) discontinuous dynamic recrystallization near twins and dislocations; (d) discontinuous dynamic recrystallization at the edge of the lamellar colony.

Fig. 5(a) shows a TEM image at the boundary between a region of equiaxed grains and a region of lamellae; the EDS map of Al is shown in the lower left corner of the figure. The bright contrast region was the γ phase, the dislocations were mainly produced in the γ grains and γ lamellae, the dislocation density was low, and no dislocations were observed in the α_2 lamellae. Figure (b) shows a TEM image of equiaxed grains, and the EDS map of Al is shown in the lower left corner of the figure. The dark contrast region was α_2 phase, and the light contrast region was the γ phase. The dislocation density in the γ grain was low, and there were only a few dislocations in the α_2 grain, which hardly contributed to the deformation of the alloy. Fig. 5(c) shows an image of another domain of equiaxed grains in the alloy, grains A and B formed

near twins and dislocations, and no dislocations were observed in the newly formed grains. These grains were formed by nucleation and growth during the tensile process, so the process was discontinuous dynamic recrystallization (DDRX). In addition, new grains produced by DDRX were observed at the edge of lamellar colony, as shown in grain C in Fig. 5 (d). The new grains were produced by transforming lamellae. The formation of grain C broke the lamellae, and grains D, E, F and G formed. Similar to the nucleation mechanism near dislocations and twins, the phase boundary had many defects with high energy, which was ideal for nucleation by DDRX. The subgrains formed by DDRX had low distortion energies, which continuously pushed the subgrain boundary outwards to reduce the distortion energy of the alloy system [22]. This was also the main reason for the low KAM value of the alloy after tensile fracture under this condition.

Fig. 6 shows TEM images of the alloy near a fracture after tensile fracture at 800 °C. Fig. 6(a) shows an image of the equiaxed grains of the alloy. As shown in the black box in the figure and the enlarged view in the upper right corner, relatively dense dislocations and dislocation arrays formed in γ grains, this provides favorable conditions for dynamic recovery (DRV). Fig. 6(b) shows another region of the alloy near the fracture. A hexagonal dislocation network (region A) and a quadrilateral dislocation network (region B) formed at the inner boundary of the grain, and similar images have been reported in other literature [23]. The dislocation moved around the grain boundary and reacted with the dislocation network, making the dislocation climb, which shows that the alloy had undergone DRV.

3.4. Deformation characteristics of alloys in the ductile stage

Fig. 7 shows an SEM image of the forged TiAl-Nb alloy after tensile fracture at 840 °C. The microstructure of the alloy after tensile fracture was composed of equiaxed grains and residual lamellae. The presence of residual lamellae was related to the plastic anisotropic properties of lamellar colonies. The volume fraction of the equiaxed grains was large, and many holes were observed in the region with equiaxed grains.

Fig. 8 shows the EBSD analysis of the region of equiaxed grains in the forged TiAl-Nb alloy after tensile fracture at 840 °C. Fig. 8(a)-(b) shows the IPF+ grain boundary map and phase map of the alloy. After tensile fracture at 840 °C, the γ grains of the alloy were heterogeneous in size, obvious refinement and spheroidization occurred, and the orientation difference between grains was large, which was attributed to the dynamic recrystallization and rotation of γ grains during the tensile process. There were many grain boundaries with small angles (shown as white lines in Fig. 8(a)) in the large γ grains, approximately 56.6%, this indicated that dynamic recovery intensified at higher temperatures. However, higher temperatures also provide a greater driving force for dynamic recrystallization and led to repeated and more adequate dynamic recrystallization. The IPF map of the α_2 phase in the alloy is shown in Fig. 8(c). After tensile fracture at 840 °C, the α_2 phase in the

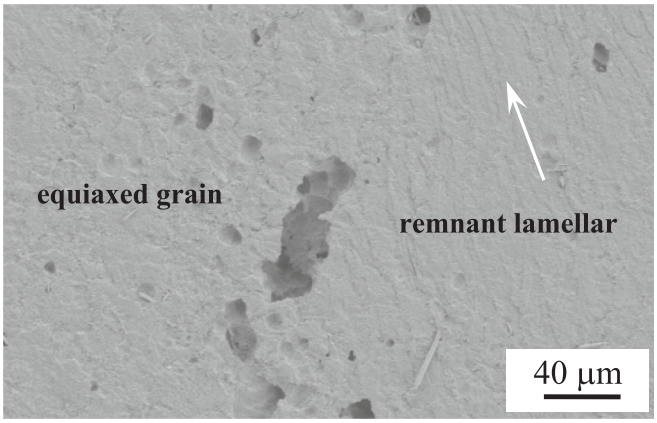

Fig. 7. SEM observations of the forged alloy near a fracture after tensile fracture at 840 °C.

equiaxed gain region was transformed into near-equiaxed grains, which were then transformed into smaller grains through dynamic recrystallization. Fig. 8(d) shows the KAM+ grain boundary map of the alloy. The KAM value of the sample after tensile fracture was significantly larger than for tensile fracture at 780 °C. The KAM values in the equiaxed grains were unevenly distributed and the large KAM value in α_2 grains indicated that the lattice distortion in α_2 grains was large.

Fig. 9 shows EBSD images of the residual lamellar region of the forged TiAl-Nb alloy after tensile fracture at 840 °C. Figs. 9(a) and Figs. 9 (b) show the IPF+ grain boundary map and phase map of the alloy, respectively. After tensile fracture at 840 °C, more γ grains appeared in the small lamellar colony, which destroyed their integrity and made the small lamellar colony decrease in size or even disappear, as shown by the black arrows in Fig. 9(a) and Figs. 9(b). The large lamellar colony showed obvious bending deformation, and the γ lamellar showed obvious coarsening, as shown by the white arrow in the figure. Small-angle grain boundaries were observed in both the equiaxed grain region and lamellar region, and the proportion of small-angle grain boundaries was approximately 35.9%. The equiaxed grains around the lamellae were heterogeneous in size and orientation. Fig. 9(c) shows the KAM map of the alloy, which showed a large KAM value. The KAM value in the α_2 lamellae was very high (shown in red), indicating that the lattice distortion in the α_2 lamellae was large during ductile fracture. The KAM values in the equiaxed grains were unevenly distributed, with higher KAM values in the smaller grains and lower KAM values in the larger grains.

Fig. 10 shows TEM images of the fracture area of the alloy after tensile fracture at 840 °C. Fig. 10 (a) shows an area of smaller lamellae and equiaxed grains. Some lamellae dissolved, and the dislocation densities in the regions with dissolved lamellae were low, such as region

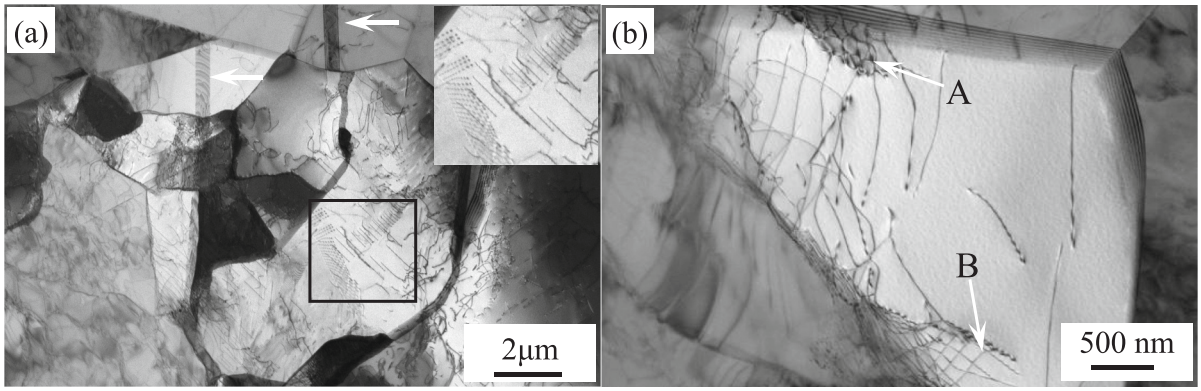

Fig. 6. Deformation features of the forged alloy at 800 °C: (a) region with equiaxed grains and (b) dislocation network at the inner boundary of the grains.

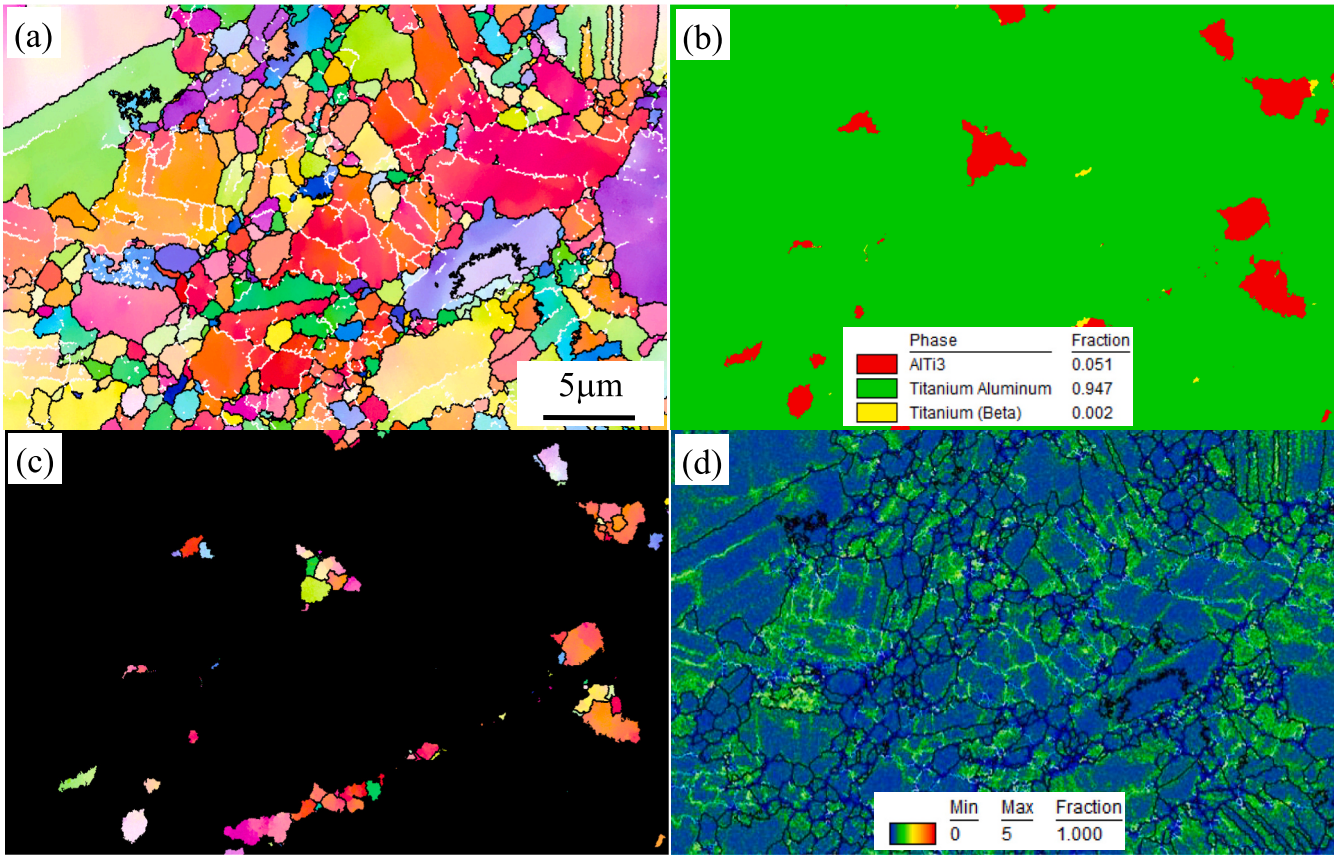

Fig. 8. EBSD observations of the forged alloy near a fracture after tensile fracture at 840 °C: (a) IPF+ grain boundary map; (b) phase map; (c) IPF map of the Ti3Al phase; (d) KAM + large-angle grain boundary map.

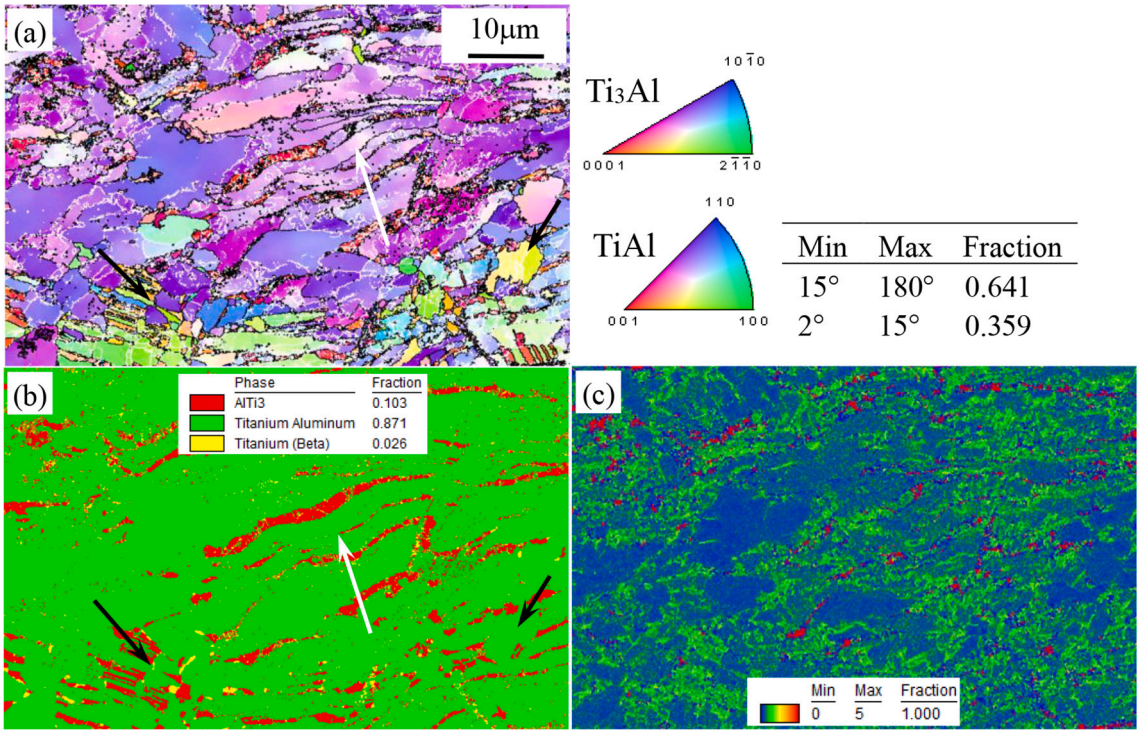

Fig. 9. EBSD observations of another area of the forged alloy near a fracture after tensile fracture at 840 °C: (a) IPF+ grain boundary map; (b) phase map; (c) KAM map.

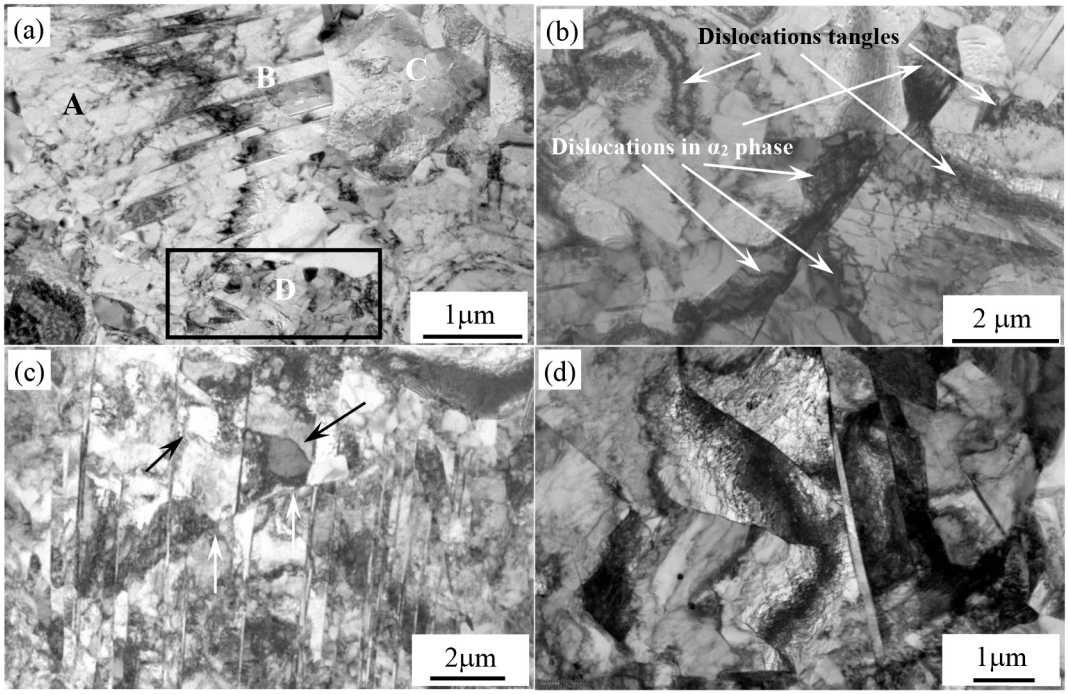

Fig. 10. Deformation features of the alloy after tensile fracture at 840 °C: (a) an area of smaller lamellae and equiaxed grains; (b) dislocation tangles; (c) coarsened lamellae; (d) rotated lamellae.

A. The dislocation densities in the residual lamellae were relatively high, as shown in region B. This indicated that a phase transition occurred during deformation at high temperature where $\alpha_2 + \gamma \rightarrow \gamma$, α_2/γ lamellae transformed into γ grains, and some of the dislocations were consumed. This process provided a softening mechanism for the deformation of the alloy in the ductile stage. Region C was a large equiaxed grain. The dislocation in the grain increased with increasing strain, which provided a driving force for the dynamic recrystallization of the alloy. Local areas broke into small grains, as shown by region D in the black box. Fig. 10 (b) shows a TEM image of the region in the alloy with equiaxed grains. Many cellular substructures formed by dislocation entanglements were observed in the ductile deformation stage. The cellular substructure divided the region of γ grains into several regions with low dislocation densities, which was the main reason for refinement of equiaxed grains. It can be seen that in this stage, the substructure forms a large angle grain boundary through absorption dislocation, and continuous dynamic recrystallization (CDRX) occurs in the alloy. In addition, some dislocations were observed in the α_2 phase, indicating that the α_2 phase also played a role in deformation during the ductile stage. Fig. 10 (c) shows a TEM image of a large lamellar colony area. The lamellae on the right side were not coarse, and obvious dislocation entanglement was observed near the lamellar area. The lamellae on the left obviously coarsened, and recrystallized grains were observed in the coarsened lamellae, as shown by the black arrow in the figure. Some lamellae broke and formed a staggered arrangement, as shown by the white arrow in the figure. Figure (d) shows that the coarsened lamellae rotated and formed irregular grains.

4. Discussion

The analysis showed that the brittle-ductile transition temperature of the forged alloy was between 800 °C and 820 °C. At brittle stage (780 °C) stage, the microstructure of the alloy did not change significantly, the main deformation mechanism of the alloy is dislocation movement and dynamic recovery (DRV) in the γ grains, α_2 phase hardly contributed to the deformation of the alloy. It is noteworthy that new grains produced by DDRX were observed in the γ grains and at the edge of lamellar colony. In the equiaxed gain region, DDRX occurred near the dislocations and twins. In the lamellar colony region, DDRX occurred at the edge of the lamellar colony. Both DRV and DDRX consumed dislocations and reduced the dislocation density in γ grains and γ lamellae, provide softening mechanism for the alloy. However, due to the short tensile time, there were fewer grains produced by DDRX in the γ grains, and the grains produced by DDRX at the edge of the lamellar colony could not destroy the integrity of the lamellar colony, so the influence on the deformation mechanism of the alloy was not obvious. In conclusion, the deformation mechanism of the alloy during the brittle stage (780 °C) included dislocation movement, dynamic recovery (DRV) and discontinuous dynamic recrystallization (DDRX) in γ grains and γ lamellae. Among them, dislocation movement and DRV was the dominant mechanism, DDRX was a secondary mechanism of alloy.

As the tensile temperature rises from 800 to 820, the yield stress strength of the alloy decreased from 516 Mpa to 400 Mpa, the elongation increased from 3.6% to 42.8%. The alloy had low resistance to deformation, which improved the hot working of the alloy. After tensile fracture, the alloy transformed into a mixed structure composed of residual lamellae and equiaxed grains. Compared with the brittle stage, the grain size of equiaxed gains is greatly reduced through repeated recrystallization. For equiaxed gains, both γ grains and α_2 grains were refined, α_2 grains underwent refinement and spheroidization and transformed into finer equiaxed grains. For lamellar colony, smaller lamellar colonies transformed into γ grains by phase transformation and further into fine γ grains by recrystallization. In the larger lamellar colonies, the α_2 lamellae underwent large bending deformation, and the γ lamellae transformed into fine grains by coarsening, recrystallization, crushing and rotation. Analysis shows that higher temperature and larger strain improved the mobility of the interface, increased the activation of the slip system of the dislocations, increased the dislocation density, and enhanced the role of DRV. Furthermore, that higher temperature provided sufficient driving force for CDRX. The fine equiaxed grains improved the plasticity of the alloy by increasing the ability of grain boundaries to slide during the high-temperature tensile process. In addition, the ability to undergo deformation was better for equiaxed grains than lamellar colonies, and thus small equiaxed grains and

domains with large volume fractions of equiaxed grains coordinated the deformation of the alloy structure and increased the plasticity of the alloy. The equiaxed grains were weaker than the lamellar colony, and thus the yield strength was less in the ductile stage.

In conclusion, the transition from lamellar colonies to equiaxed grains and the refinement of equiaxed grains were the main reasons for the brittle-ductile transition.

5. Conclusions

1) The original structure of the forged high Nb-TiAl alloy was composed of lamellar colonies and equiaxed grains. The temperature for the brittle-ductile transition of the alloy was between 800 °C and 820 °C.
2) After tensile fracture in the brittle stage, the microstructure of the alloy was still a mixture of lamellar colonies and equiaxed grains. The main deformation mechanism of the alloy was dislocation movement and DRV in γ grains and γ lamellae.
3) After tensile fracture in the ductile tensile stage, the microstructure of the alloy changed into a mixture of residual lamellae and equiaxed grains. The main deformation mechanisms of the alloy were continuous dynamic recrystallization (CDRX) and lamellar fragmentation. In addition, the phase transition had a great influence on the deformation ability of the alloy.

Declaration of Competing Interest

The authors declare that they have no known competing financial interests or personal relationships that could have appeared to influence the work reported in this paper.

Data availability

No data was used for the research described in the article.

Acknowledgements

This work was supported by the Science And Technology Project of Bijie City (bikelianhe[2023]36, bikelianhe[2023]9, bikelianheziG [2019]8, bikelianhe[2023]37), Natural Science Research Project of Guizhou Higher Education Institutions of China (QJJ [2023]047), Sanke (2022002005), Doctoral Research Start-up Fund of Liaoning Province (2023-BS-195), Basic Scientific Research Project of Department of Education of Liaoning Province (LJKMZ20220960), Coal & Phosphorus Chemical Engineering Technology Center of Bijie City ([2015]1) and Characteristic Key Laboratory of University of Guizhou Province (qianjiaoheKYzi [2019]053).

References

[1] Z.K. Yin, J.S. Chen, P.L. Zhang, et al., Phase stability, brittle-ductile transition, and electronic structures of the TiAl alloying with Fe, Ru, Ge, and Sn: a first-principle investigation, J. Mol. Model. 26 (11) (2020) 1–12.
[2] A. Raina, Volume dependent fracture energy and brittle to quasi-brittle transition in intermetallic alloys, Eng. Fract. Mech. 264 (2022), 108312.
[3] S. Djanarthany, J.C. Viala, J. Bouix, An overview of monolithic titanium aluminides based on Ti_3Al and TiAl, Mater. Chem. Phys. 72 (3) (2001) 301–319.
[4] V.M. Imayev, A.A. Ganeev, D.M. Trofimov, et al., Effect of Nb, Zr and Zr + Hf on the microstructure and mechanical properties of β-solidifying γ-TiAl alloys, Mater. Sci. Eng. A 817 (6) (2021), 141388.
[5] S. Liu, H. Ding, R. Chen, et al., Evolution of rapidly grown cellular microstructure during heat treatment of TiAl-based intermetallic and its effect on micromechanical properties, Intermetallics 132 (2021), 107166.
[6] H. Liu, Q. Wang, J. Zhang, et al., Effect of multi-pass deformation on hot flow behavior and microstructure evolution mechanism of Ti-6Al-4V alloy fabricated by hot isostatic pressing, J. Mater. Res. Technol. 17 (2022) 2229–2248.
[7] S. Yim, H. Bian, K. Aoyagi, et al., Effect of multi-stage heat treatment on mechanical properties and microstructure transformation of Ti-48Al-2Cr-2Nb alloy, Mater. Sci. Eng. A 816 (2021), 141321.
[8] Y.W. Kim, Microstructural evolution and mechanical properties of a forged gamma titanium aluminide alloy, Acta Metall. Mater. 40 (6) (1992) 1121–1134.
[9] V.S. Sokolovsky, N.D. Stepanov, S.V. Zherebtsov, et al., Hot deformation behavior of β-solidifying TiAl based alloy, Acta Phys. Pol. A 134 (3) (2018) 675–677.
[10] J. Wesemann, G. Frommeyer, J. Kruse, Microstructure and mechanical properties of an extruded γ-TiAlMoSi alloy, Intermetallics 9 (4) (2001) 273–278.
[11] Y.Y. Chen, Y.F. Chen, F.T. Kong, et al., Fabrication and processing of gamma titanium aluminides -a review, Mater. Sci. Forum 638-642 (2010) 1281–1287.
[12] H. Clemens, H. Kestler, Processing and applications of intermetallic γ-TiAl-based alloys, Adv. Eng. Mater. 2 (9) (2000) 551–570.
[13] G.A. Salishchev, R.M. Galeyev, O.R. Valiakhmetov, et al., Highly superplastic Ti-6Al-4V sheet for superplastic forming and diffusion bonding, Mater. Technol. 15 (2) (2000) 131–142.
[14] F. Qiang, E. Bouzy, H. Kou, et al., Grain fragmentation associated continuous dynamic recrystallization (CDRX) of hexagonal structure during uniaxial isothermal compression: high-temperature α phase in TiAl alloys, Intermetallics 129 (2021), 107028.
[15] C. Shi, K. Zhang, S. Jiang, et al., Pulse current auxiliary forging of sintered TiAl alloys based on the investigation of dynamic recrystallization and phase transformation, Mater. Charact. 135 (2017) 325–336.
[16] N. Cui, Q. Wu, K. Bi, et al., Effect of multi-directional forging on the microstructure and mechanical properties of β-solidifying TiAl alloy, Materials 12 (9) (2019) 1381–1392.
[17] S. Bystrzanowski, A. Bartels, A. Stark, et al., Evolution of microstructure and texture in Ti-46Al-9Nb sheet material during tensile flow at elevated temperatures, Intermetallics 18 (5) (2010) 1046–1055.
[18] V.M. Imayev, R.M. Imayev, G.A. Salishchev, On two stages of brittle-to-ductile transition in TiAl intermetallic, Intermetallics 8 (1) (2000) 1–6.
[19] Y.M. Tan, H.Z. Fang, R.R. Chen, et al., Microalloying effects of ho on microstructure evolution and high temperature properties of Ti46Al4Nb1Mo alloy, Intermetallics 126 (2020), 106883.
[20] Q. Wang, R.R. Chen, D.Z. Chen, et al., The characteristics and mechanisms of creep brittle-ductile transition in TiAl alloys, Mater. Sci. Eng. A 767 (2019), 138393.
[21] H.Z. Niu, Y.Y. Chen, S.L. Xiao, et al., High temperature deformation behaviors of Ti-45Al-2Nb-1.5V- 1Mo-Y alloy, Intermetallics 19 (12) (2015) 1767–1774.
[22] H. Zhou, F. Kong, X. Wang, et al., Hot deformation behavior and microstructural evolution of as-forged Ti-44Al-8Nb-(W, B, Y) alloy with nearly lamellar microstructure, Intermetallics 81 (2017) 62–72.
[23] A. Couret, H.A. Calderon, Patrick Veyssière, Intralamellar dislocation networks formed by glide in γ-TiAl I. the mechanism of formation, Philos. Mag. 83 (14) (2003) 1699–1718.